Int. J. Multiphase Flow, Vol. 3, pp. 561–583. Pergamon/Elsevier, 1977. Printed in Great Britain

BOUNDARY-ENHANCED SEDIMENTATION DUE TO SETTLING CONVECTION

W. D. HILL,* R. R. ROTHFUS and KUN LI
Department of Chemical Engineering, Carnegie-Mellon University, Pittsburgh, PA 15213, U.S.A.

(*Received* 13 *September* 1976; *received for publication* 6 *April* 1977)

Abstract—Sedimentation rates are significantly enhanced when the process occurs in containers of certain shapes or orientations. For example, sedimentation in a conical vessel or a tilted tube may be several times faster than sedimentation in a vertical tube of the same height. This enhancement results from a naturally occurring convection.

Monodisperse particles were observed during settling from a viscous, incompressible, and Newtonian fluid contained beneath an upward-pointing cone. At particle concentrations of about 0.05 per cent by volume, convective velocities reach ten times the particle settling velocity, and sedimentation is complete in 40 per cent of the time necessary in a vertical tube.

Continuum fluid mechanics successfully models this settling convection. The mechanism is particle momentum transfer to fluid. The model requires numerical solution but its functionality can be investigated in terms of dimensionless parameters.

INTRODUCTION

Studies in many fields have reported enhanced sedimentation resulting from a naturally occurring convection. This "settling convection" has been observed during batch sedimentation in certain enclosure geometries. The mechanism responsible for this phenomenon has never been demonstrated.

Mechanisms can be postulated and worked into models of settling convection, but confirmation of any such model requires that its prediction be compared to fundamental data from an observable case. Convective velocities are observed in this work for a simple, two-dimensional case of settling convection. These, the first observations of their kind, serve to confirm a model and thus the mechanism on which it is based.

Confirmation of the mechanism permits predictive modeling and the interpretation of the ruling dimensionless parameters. This study makes an important start toward functionality as the basis of criteria for the design of settlers employing settling convection.

PREVIOUS WORK

The phenomenon of settling convection has been primarily studied for the case of settling in inclined tubes. Boycott (1920) observed the sedimentation of corpuscles in test tubes containing blood and discovered that a greater percentage of corpuscle-free fluid appeared with sedimentation time in inclined tubes than in vertical tubes.

Mechanistic explanations of settling convection have been proposed. Lundgren (1927, 1928) proposed that an explanation for Boycott's effect lay in the ability of liquid displaced by settling particles to bypass percolation back up through the dense cloud of falling particles by flowing upward beneath the upper inclined surface. Kinosita (1949) observed convection currents during sedimentation in tilted tubes and beneath inclined boundaries. He proposed that these currents account for Boycott's curiosity. He observed some particles to move at 100 times their sedimentation velocity.

Several models of settling convection have been presented, but none has a true mechanistic basis. Each model contains an assumption of interface shape. Each predicts only interface

Presented in part at the A.I.Ch.E. 68th Annual Meeting.

*Present address: E. I. du Pont de Nemours & Co., Inc., Industrial Chemicals Department, Experimental Station B336, Wilmington, DE 19898, U.S.A.

movement, accelerating the movement as the result of hypothetical flows of clear fluid out from suspension situated beneath an inclined surface to join clear fluid above the interface.

Derivation of the first model is generally attributed to Nakamura & Kuroda (1937) but was in fact preceded by the similar, but less developed model of Ponder (1925). The model is derived for sedimentation in an inclined, rectangular tube resting on a bottom edge as shown in figure 1. The tube of side length A and inclined at an angle Ω to the vertical is initially filled with a uniform slurry to vertical height $B + A \cdot \sin \Omega$. Approximating behavior observed for certain suspensions (all experiencing hindered settling), the suspension interface is constrained to be a horizontal plane located a distance $h(t)$ beneath the liquid surface as a function of time, t. It is argued that in a time dt unconstrained particles would all fall a distance $s \cdot dt$ (where s is their settling velocity in a vertical tube) and the clarified volume should increase as illustrated by the arrows. No clarified volume is observed to exist along the upper inclined surface, however. The model postulates that this clarified liquid be added to the clarified liquid above $h + s \cdot dt$, giving the observed increase of h to $h + dh$ in time dt.

The resultant prediction for $h(t)$ is

$$h = (B + A \sec \Omega)\left[1 - \exp\left(\frac{-st \sin \Omega}{A}\right)\right]. \qquad [1]$$

This equation apparently represents an upper limit to the rate of sedimentation. Later workers, including Graham & Lama (1953) and Vohra & Ghosh (1971), found less enhancement of sedimentation than predicted by the equation and have inserted empirical coefficients into the equation.

Recently Zahavi & Rubin (1975) have presented a more complicated model which assumes a horizontal interface coupled with a thin clear layer beneath a vessel's downward-facing inclined surfaces. The model requires both an empirical constant, determined for the enhanced-sedimentation effect of a given fluid/particle system, and settling rate versus concentration data for vertical vessels. The empirical constant is assumed to represent a fixed average rate of clear fluid generation per unit area of downward-facing, inclined surface in the suspension.

The solids concentration at the horizontal interface is assumed to vary in inverse proportion to the area of the interface. When vessel shape dictates that the area of the interface changes during sedimentation, the resultant change in particle concentration at the interface is taken to affect the rate of settling of interface particles. Interface movement is based on this concentration dependent rate of interface settling, further increased to allow for the clear fluid generation under inclined surfaces. A match between the model and data of Zahavi & Rubin (1975) may be explained by the amount of empirical correlation involved.

Oliver & Jenson (1964) have presented a model in which the assumed interface, shown in figure 2, was a function of two parameters, h and e. Such interface shapes were observed in using monodisperse polymer suspensions of 1–15 per cent by weight. The model was developed

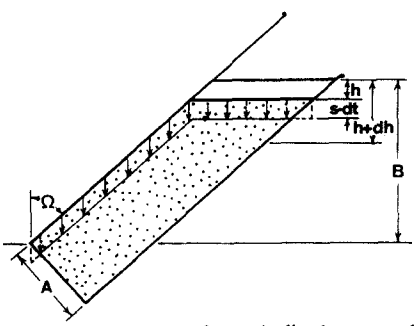

Figure 1. PNK theory for an inclined, rectangular settling tube.

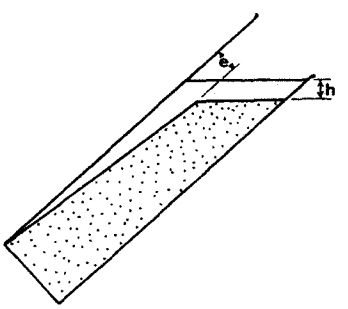

Figure 2. Oliver and Jenson theory for an inclined, rectangular settling tube.

from the implied dynamic geometry and the addition of a simple convection term containing an empirical function of concentration and angle of inclination. The solution, giving the two parameters as a function of time, was obtained on an analog computer. Agreement between the model and data was fair.

As in the work reviewed above, this paper presents a model for settling convection in the context of the batch sedimentation of an initially uniform and quiescent suspension in a vessel without a single, horizontal upper-bound. It should be noted, however, that there are other contexts in which similarly based convection is observed. Pearce (1921) first saw a relationship between inclined baffles in clarifiers (recently touted in the form of "high-rate settlers") and inclined tube sedimentation. Convection has been noted as a source of error in sedimentation size analysis by Coutts & Crowther (1925) and Kast (1960). The settling of particle clouds is enhanced by convection (Woodward 1964) and geological significance has been ascribed to this fact (Bradley 1965). Such convecture phenomena have in several instances, been ascribed to momentum transfer from particles to fluid.

EXPERIMENTAL STUDY

Preliminary consideration

Based upon the literature, three mechanisms can be postulated as causing settling convection: (I) suspension density gradients, allied with particle concentration gradients, are not parallel to hydrostatic pressure gradients. Convection acts toward establishing a downward gradient of density. (II) Return flow of liquid displaced by settling particles channels through regions of lower particle concentration. (III) Particles collect near, and flow down along, upward-facing, inclined surfaces (where such a surface is present).

On the hypothesis that mechanism I is the dominant cause of settling convection, experiments were designed in which the other mechanisms could not account for significant convection. Working at low volumetric particle concentrations (~0.05 per cent) causes return flow to be negligible and rules out mechanism II. Mechanism III is eliminated by studying sedimentation beneath an upward-pointing cone where there are no *up*ward-facing, inclined surfaces.

In contrast to the case in enclosures previously studied, batch sedimentation in an upward-pointing cone is a predictably two-dimensional phenomenon. The suspension interface has the same shape in all radial planes. Fluid and particle velocities are confined to radial planes.

Considering that the phenomenon is convective in nature, observation is focused on particle motion. But the particle motion in a radial plane of a cone must be viewed through a depth of undisturbed suspension. Particles of a small size relative to the enclosure will, at all but unacceptably dilute concentrations, mask observation of a radial plane. This problem is averted by use of a matched-refractive-index, fluid/particle system which is optically more dilute than it is in fact. If the majority of the particles are transparent, they are invisible in a fluid of matching refractive index. An adjustable minority of non-transparent particles are dispersed as the visible constituent of the suspension.

Fluid/particle system

Properties of the fluid/particle system are tabulated in table 1. The particles are glass beads sieved into narrow size ranges.

The necessary non-transparent particles were manufactured from the clear beads by a fine surface silvering. An old mirror silvering process was adapted to the purpose from its description by Strong (1938, p. 157). The resultant silvered "markers" were virtually identical to the parent, clear beads in all but optical properties. The volume fraction of markers in suspension was set at 2.5×10^{-5} or 1.5×10^{-5} for size range I or size range II respectively.

In green light and at 30°C the refractive index of the clear beads matched that of a mixture of two hydrocarbon oils. The major constituent of the fluid mixture was Monsanto HB-40, a 40 per cent hydrogenated terphenyl. This constituent possesses an unusually high ratio of

Table 1. Summary of experimental matched refractive index system (30°C, 550 nm)

Glass beads		
Shape, 99.9 per cent spherical, very few voids.		
Size distribution after sieving:		
	Size I	Size II
mean diameter ($P = 0.95$)	$132.0 \pm 0.5\ \mu m$	103.2 ± 0.4
standard deviation	$6\ \mu m$	$1.8\ \mu m$
range containing 75 per cent	$123–139\ \mu m$	$101–105\ \mu m$
Composition, Corning code 0221, 1–1–3 parts, soda–lime–silica by wt		
Color, clear		
Refractive index, 1.547		
Density, 2.65 g/cm^2		
Fluid		
Composition, 79.30 per cent by wt. hydrogenated terphenyls (Monsanto HB-40®)		
20.70 per cent heavy mineral oil (Fisher 0-120)		
Color, yellowish, clear to 550 nm light		
Refractive index, 1.547		
Density, 0.970 g/cm^2		
Viscosity, 36.0 centipoise (0.036 N · sec/m^2)		
Fluid/particle system		
Particle concentration, around 0.05 per cent by volume (dilute!)		
Fraction silvered markers, commonly 0.05		
Particle Reynolds No, (I) 0.00149; (II) 0.000707 (laminar)		
Settling velocity, (I) 0.046 cm/sec; (II) 0.025 cm/sec		

refractive index to density and is easily handled. The refractive index was lowered to the matching value by dilution with a heavy, white mineral oil.

Fluid/particle properties combine to give a simplified behavior. Settling occurs at low Reynolds number, Brownian motion is negligible, and coagulation of particles is minimal.

Particle settling velocity is a particularly important system property in this work. For this reason empirical settling-velocity distributions were obtained for each of the bead size fractions using silvered beads at 0.0025 per cent by volume in the chosen fluid. Other than use of a vertical-walled settling enclosure, the technique used to measure settling velocities was identical to the technique used for measuring particle velocities during an experimental run (technique detailed later). The empirical distributions for size fractions I and II were approximately normal with means of 0.0461 ± 0.0007 cm/sec and 0.0251 ± 0.0005 cm/sec respectively and standard deviations of 0.0037 cm/sec and 0.0026 cm/sec respectively. The empirical distributions were broader than distributions calculated from particle size ranges and other measured physical properties using Stokes' law, but the means of the empirical and calculated settling velocities agreed within 7 per cent for both size fractions.

Apparatus

The conical enclosure was provided by one of two glass funnels inverted on a plate. They had an internal base diameter of 14.0 cm and base angles of 59.7° and 47°C. The funnel tubes at the top of the cones were 1.4 cm in diameter.

An open-top, rectangular "cell" or tank was constructed to contain the fluid/particle system. Agitation was carried out in this cell, and then a cone was immersed and set on the bottom of the cell. Glass walls in the cell provided an undistorted view into fluid under the cone.

Initial agitation of the suspension was provided by cyclic vertical movement of a horizontal, perforated plate within the fluid. The cone was inserted into the rectangular cell on top of the perforated plate following complete particle dispersion. The final step of the agitation was to raise the perforated plate to the surface of the fluid while the cone was positioned on it and then to lower the two together back to the base of the cell.

Zero experimental time was defined as the moment that agitation ceased. There were uncertainties in the state of the system at this time. Ideally the suspension was to have been

well-mixed and quiescent. Deviation from this state was, to a degree, experimentally examined. The use of tracers showed that at 15 sec, the earliest practical time of observation, all residual velocities in a normally agitated, fluid-filled cone were less than 0.005 cm/sec. The uniformity of initial particle dispersion was inferred from the photographic observation of particle dispersion in two separated regions after 15 sec of sedimentation. A statistical analysis showed good probability that the distribution of local particle concentration within the two regions came from one and the same Poisson distribution.

Thermal convection in the system was eliminated by careful temperature control of the rectangular cell and the cone at 30.0 ± 0.1°C.

Observations were restricted to the vicinity of a radial plane in the cone by photomacrographic camera optics. Only particles within ~0.1 cm of the subject plane were in focus. Photographs were produced at three-fold magnification on 4 in. × 5 in. Polaroid film. Each photograph covered only about two square inches of the subject plane. For study on the larger cone scale, a montage of photographs from *different* runs under *identical* conditions was assembled. Successful assembly was practical because of good experimental reproducibility and an accurate photographic positioning mechanism (±0.2 cm in both vertical and horizontal directions).

Particle motion was photographically recorded as a multiexposure by exposing each film while the subject area was illuminated with a precisely timed sequence of strobe flashes. The sequence was flash/1 sec pause/flash/1 sec pause/flash/1 sec pause/flash/2 sec pause/flash/1 sec pause/flash. The sequence was assymmetric in time, so that direction of movement was indicated. The fourth, central flash occurred at what was defined as the nominal observation time. Particle velocities and accelerations at this time could be easily approximated from the multiexposured images of each particle.

Light was collated, filtered to pass only green light (~60 per cent, 520–575 nm), and directed obliquely from the camera side toward the subject area.

Observations

Settling convection was studied in the most detail for the "standard" case of the sedimentation of a 0.05 volume per cent suspension of size fraction I beads beneath the 59.7° cone. Montage photographs of particle motion were collected for 15, 30, 45, 60, 75, 90, 105, 120 seconds of sedimentation.

Plots derived from the first four of the montages are shown in figures 3–6. Particle motion in the montages was represented by small light images on a gray background, and thus the montages can not be easily reproduced (reproductions are on record in Hill (1974)). Particle motion in the derived plots is represented by sets of black dots and these are displayed for only a small fraction of the particles appearing in the original montages. One particle's motion is represented by a series of six dots representing the multiexposure of particle position over 6 sec. During the first 3 sec, the particle travelled between the four adjacent dots and in the second 3 sec travelled on to the fifth and sixth dots.

The standard case is dramatically different from sedimentation in a vertical-walled vessel where particles settle vertically at a uniform rate. Rather, particles are swept up by a strong counter-clockwise circulation which develops early in the sedimentation. Particles in the vicinity of the cone centerline settle much faster than is accountable by their Stokes velocities. The uppermost particles move quickly downward, tending to level out the top of the cloud of particles (the upper interface). As particles approach the base, they angle radially outward toward the cone walls, thus maintaining substantial base coverage by the cloud of particles. Particles near the cone walls and removed from the base are convected upward!

The convection is vigorous and effective in reducing settling time. At 30 sec some particles are moving at over eight times their experimentally-confirmed Stokes velocities. Sedimentation is completed in 40 per cent of the time necessary in an equal-height, vertical tube.

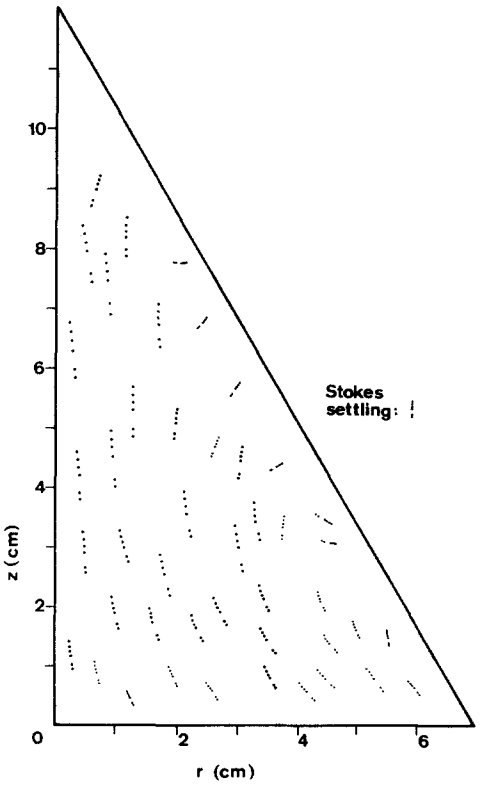

Figure 3. Settling time, 15 sec.

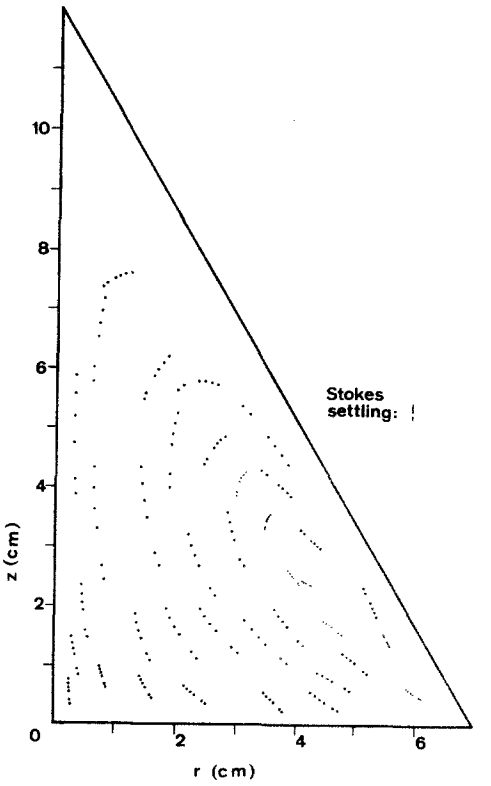

Figure 4. Settling time, 30 sec.

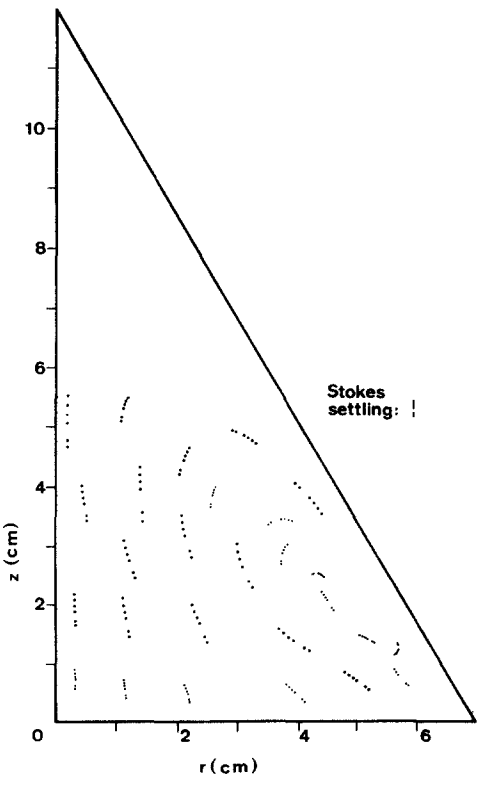

Figure 5. Settling time, 45 sec.

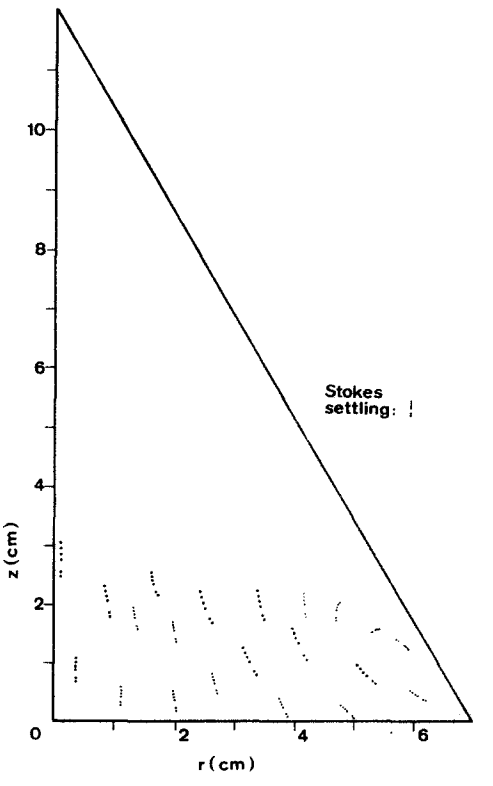

Figure 6. Settling time, 60 sec.

Figures 3–6. Observed particle trajectories for standard case (0.0005 volume fraction particles of size fraction I, in cone with 59.7° base angle).

Variations on the standard case were examined through three independent parameters: particle concentration, particle settling velocity, and cone base angle. A collection of montages were produced to follow the sedimentation in each case where a parameter was varied. For each manipulated parameter, the particle motion represented in one such montage is presented later in this paper in a direct comparison with predicted particle motion (figures 14–16). In each case of convection, the character of the circulation was the same.

Particle concentrations of virtually zero and of 0.20 volume per cent were examined for comparison with the standard-case level of 0.05 volume per cent. At particle concentrations approaching zero, all particles settle at their Stokes velocities. At the highest concentration studied, the particle cloud was more quickly leveled than in the standard case, but sedimentation was completed only slightly sooner. Figure 14 shows particle motion after 60 sec of settling at this concentration.

Sedimentation of the smaller, size-fraction II beads dispersed at the standard particle volume fraction was also studied. Figure 15 shows particle motion at 60 sec. The time scale of the sedimentation was lengthened in approximately inverse proportion to the settling velocity of the particles. The particle cloud was, however, more leveled at a given degree of particle removal when the smaller particles were used.

Sedimentation of the standard fluid/particle system was studied beneath the alternative cone with a 47° base angle. The process was completed more quickly than in the standard case, but this was nearly accounted for by the relative height of the cones. Particle motion at 30 sec is shown in figure 16.

Analysis

One serious shortcoming of the experimental technique was that suspension interfaces were not conclusively defined in the montages. Interface placement for purposes of analysis was a matter of personal judgement and thus not very useful. Figure 7 presents an average of two

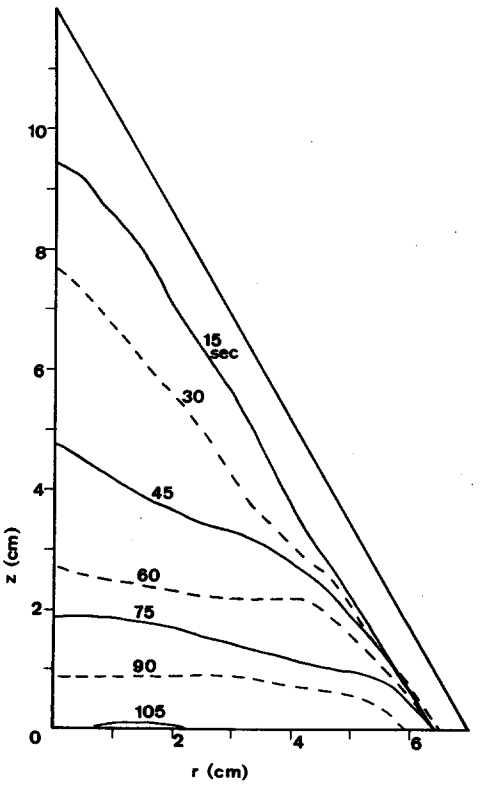

Figure 7. Interface positions estimated from observation of the standard case.

individual judgements of the position of the experimental interface during settling of the standard case.

Accurate data on particle velocities, however, was available from the montages. Each "observed" particle velocity represented a time-average over 6 sec of particle motion, and, as such, was accurate to within 0.002 cm/sec. The velocity was identified with the time-average particle position. Over 600 velocity/position data sets were collected and are available elsewhere (Hill 1974). They may be used to check the validity of a mechanistic model.

Obviously, a new model is needed because none of the past models have derivations consistent with the convective mechanism observed here. None allow for any concentration dependence, at least at the low concentrations employed here. That is, they do not extrapolate to unenhanced sedimentation at zero concentration. Each of the previous models predicts that at $t = 0$ the suspension interface in a cone is falling with an infinite velocity.

By confirming the presence of significant settling convection at low concentrations and beneath a cone, the experiments have restricted the list of possible mechanisms.

THEORETICAL MODEL

Mathematical representation

A monodisperse slurry of small particles may be treated as two interacting continua—an extended, homogeneous fluid and a homogeneous particle "cloud". True point variables are replaced by smoothed variables obtained by averaging over regions which are large compared with particle spacing but small compared with the complete system. The smoothed variables for one phase are "reduced" to continuously fill the system.

There have been many derivations of somewhat-general continuum models consisting of sets of complex partial differential equations. It is possible to start from these complex forms, and with appropriate approximation, reduce them to the model which is presented here. The general formulation of Soo (1967) was reduced under the following assumptions: (1) the system is two-phase, non-reactive, and isothermal. (2) One phase consists of monodisperse, spherical, rigid particles. (3) The second phase is an incompressible and Newtonian fluid. (4) Particles are in dilute suspension in the fluid. (5) Gravity is the only active body force. (6) Relative motion between phases is laminar and at quasi-steady state.

The resultant equations, most conveniently presented in dimensionless form, include a fluid momentum equation,

$$\frac{\partial \mathbf{V}}{\partial T} + N_{Re}\mathbf{V}\cdot\nabla\mathbf{V} = -\nabla\Theta - \frac{N_{Gr}}{N_{Re}}(1-\Phi)\hat{g} + \nabla^2\mathbf{V}, \qquad [2]$$

a fluid continuity equation,

$$\nabla\cdot\mathbf{V} = 0, \qquad [3]$$

and a particle continuity equation,

$$\frac{\partial \Phi}{\partial T} + N_{Re}(\mathbf{V}+\hat{g})\cdot\nabla\Phi = 0. \qquad [4]$$

In place of a particle-momentum equation there stands the condition that particles settle with a predetermined settling velocity relative to the fluid, i.e.

$$\mathbf{V}_p = \mathbf{V} + \hat{g}. \qquad [5]$$

Two dimensionless groups appear, a sedimentation Reynolds number and a sedimentation

Grashof number. These are defined as

$$N_{Re} = \frac{BW\rho}{\mu} \qquad [6]$$

and

$$N_{Gr} = \frac{B^3 g\rho(\rho_p - \rho)\phi^0}{\mu^2} \qquad [7]$$

where B = vertical enclosure dimension, e.g. cone height; W = particle settling velocity; ρ_p = density of particulate material; ρ = density of fluid; μ = viscosity of fluid; g = acceleration due to gravity. Direction unit vector is $\hat{g}$; and ϕ = particle volume fraction. Initial value ϕ^0.

If the particles are spheres of radius, a, and are initially separated by an average interparticle distance, l, then

$$W = \frac{2a^2 g(\rho_p - \rho)}{9\mu}, \qquad [8]$$

$$N_{Re} = \frac{2a^2 Bg\rho(\rho_p - \rho)}{9\mu^2}, \qquad [9]$$

$$\frac{N_{Gr}}{N_{Re}} = 6\pi \frac{aB^2}{l^3}. \qquad [10]$$

The dimensionless independent variables, time and space coordinates, are defined in terms of the dimensioned variables t and x_i, as

$$T = \frac{\mu}{B^2\rho} t, \qquad [11]$$

$$X_i = \frac{x_i}{B}. \qquad [12]$$

Dimensionless forms of the dependent variables, particle concentration and velocity vector, $\mathbf{v}$, are similarly defined:

$$\Phi = \frac{\phi}{\phi^0}, \qquad [13]$$

$$\mathbf{V} = \frac{\mathbf{v}}{W}. \qquad [14]$$

Dependent variable Θ is a pressure function whose dimensionless gradient is defined in terms of the gradient of a dimensioned pressure function $\nabla\theta$ and the pressure gradient ∇p by:

$$\nabla\Theta = \frac{B^2}{\mu W}\nabla\theta = \frac{B^2}{\mu W}[\nabla p - \rho g - \phi^0(\rho_p - \rho)g]. \qquad [15]$$

By this definition $\nabla\Theta$ is zero at the initial time, and solution of the equations is simplified.

The fluid motion is described by [2] and [3] which, but for the addition of the term $-(N_{Gr}/N_{Re})(1-\Phi)\hat{g}$ to the momentum equation, are those commonly used for a fluid with constant density and viscosity. The constant part of the term, $-(N_{Gr}\hat{g}/N_{Re})$, appears as a result of the introduction of Θ and causes the overall term to vanish at the initial time.

The variable part of the term, $(N_{Gr}/N_{Re})\Phi\hat{g}$, has two interpretations. In the context of the interacting continua approach, it represents the "smoothed", local momentum-transfer from settling particles to fluid. In dimensional form the group $(\rho_p - \rho)\phi g$, is seen to be the momentum transfer rate per unit volume of suspension. This part of the term may also be viewed as a reaction in the fluid to the drag forces acting on particles. Thus it is proportional to particle concentration and in the direction of gravity.

If the "fluid" momentum equation is viewed as a slurry momentum equation, then the variable part of the term takes on a Boussinesq interpretation in terms of one continuum fluid possessing the bulk slurry density. Bouyancy forces result as this density varies with particle concentration. At low particle concentration, the density difference between slurry and clear fluid may be sufficiently small that its effect on continuity and the viscous-force terms can be ignored, while its effect via the bouyancy-force term is significant. The model is applied under these conditions.

The effect of the term is that fluid containing particles will tend to flow downward relative to fluid free of particles. There will be resultant flow whenever the gradient of particle concentration is not co-directional with gravity.

The above model is compatible with the conditions prevailing in the experimentally studied case of sedimentation beneath a cone. This case is two-dimensional in the cylindrical coordinates r (radial) and z (axial from the base). The two-dimensionality was experimentally confirmed.

In cylindrical coordinates and dimensioned variables the modeling equations become

$$\frac{\partial u}{\partial t} + \frac{\partial (ru^2)}{r\partial r} + \frac{\partial (uv)}{\partial z} = -\frac{\partial \theta}{\partial r} + \frac{\mu}{\rho}\frac{\partial}{\partial z}\left(\frac{\partial u}{\partial z} - \frac{\partial v}{\partial r}\right), \tag{16}$$

$$\frac{\partial v}{\partial t} + \frac{\partial (ruv)}{r\partial r} + \frac{\partial v^2}{\partial z} = -\frac{\partial \theta}{\partial z} + \frac{\rho_p - \rho}{\rho} g\phi^0(1-\Phi) - \frac{\mu}{\rho r}\frac{\partial}{\partial r}\left[r\left(\frac{\partial u}{\partial z} - \frac{\partial v}{\partial r}\right)\right], \tag{17}$$

$$\frac{1}{r}\frac{\partial (ru)}{\partial r} + \frac{\partial v}{\partial r} = 0 \tag{18}$$

and

$$\frac{\partial \Phi}{\partial t} + u\frac{\partial \Phi}{\partial r} + (v - W)\frac{\partial \Phi}{\partial z} = 0, \tag{19}$$

where u and v are fluid velocities parallel to the r and z axes respectively. Since gravity is in the direction of decreasing z, the equivalent particle velocities are

$$u_p = u, \tag{20}$$

$$v_p = v - W. \tag{21}$$

The solution geometry of interest is a right triangle, a symmetrical half of that portion of an r,z-plane which is contained under the cone. There are three boundaries to the right triangle, the cone axis, the inclined cone surface, and the base. The axisymmetric condition along the cone axis gives

$$u = 0 \quad \text{and} \quad \frac{\partial v}{\partial r} = 0. \tag{22, 23}$$

The other boundaries are no-slip, i.e.

$$u = v = 0. \tag{24, 25}$$

The solution technique which follows does not directly require pressure boundary conditions, but these are Newman-type conditions specifying pressure gradients normal to the boundaries.

Most initial conditions are homogeneous throughout the region;

$$u = v = \theta = 0. \qquad [26, 27, 28]$$

The suspension interface initially coincides with the inclined cone surface. On this boundary

$$\Phi = 0, \qquad [29]$$

elsewhere in the region

$$\Phi = 1. \qquad [30]$$

From the viewpoint of the particle cloud, these conditions imply that particles are falling out of the system through the portion of the base which is covered by the cloud. In the dilute approximation these particles do not displace fluid and do not result in a return flow of fluid. It is also implied that the particle concentration must always be zero on the inclined cone surface.

The particle continuity equation, [19], represents a vanishing of the substantial (or "Lagrangian") derivative of particle volume fraction with respect to particle velocities. Thus, if an observer moves along with the particle phase velocity, the concentration in the vicinity of the observer can not change. The prescribed initial condition includes a sharp interface separating a region of uniform particle concentration beneath the cone from one of zero concentration above. In combination with the above Lagrangian interpretation, this directs that the moving interface will continue to be sharp and to contain a region with the initial concentration. Interface movement is defined by the movement of particles at the interface satisfying [20] and [21].

This restriction to constant concentration in the particle cloud is the result of an assumption in the derivation of the continuity equations. The more complete fluid continuity equation, from which [3] is derived, expands to give

$$\frac{\partial \Phi}{\partial T} + N_{Re}\mathbf{V} \cdot \nabla\Phi = N_{Re}(1-\Phi)\nabla \cdot \mathbf{V}. \qquad [31]$$

The L.H.S. is assumed to be negligible in comparison to the R.H.S. when the suspension is dilute. The derivation of the particle continuity equation, [4], entails this same assumption of negligible concentration change, and thus causes the restriction.

Solution technique

No analytical solution to the problem posed by the model has been found. Numerical solutions are possible using a complex finite difference scheme. The basis of the scheme employed here is the SMAC method developed by Amsden & Harlow (1970*a*,*b*) at Los Alamos.

Finite differences schemes involve judiciously representing partial derivatives by approximations based upon differences in variable value at discrete and regular positions in space and time. The right-triangular solution region of the current problem is covered by the mesh illustrated in figure 8 with horizontal mesh spacing δr and vertical mesh spacing δz. Individual cells are referenced by an integer pair (i, j) where i indicates the column counting from left and j indicates the row counting from the bottom. Variable values at discrete locations are subscript to refer to their position in the mesh, and these locations are illustrated in figure 9 for cell (i, j). The radial coordinate at the center of the ith column of cells is represented by r_i.

Time is also expressed in discrete steps, δt. Variable values are superscript to indicate the

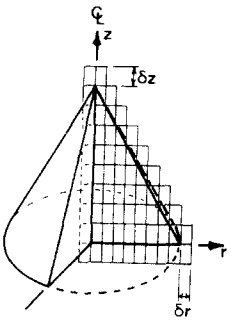

Figure 8. Computing mesh covering a radial slice in a cone.

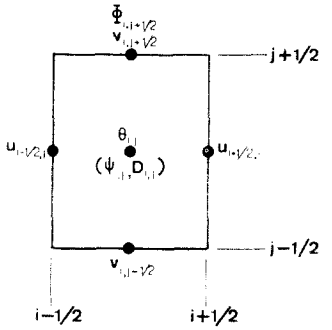

Figure 9. Variables defined in a cell of the computing mesh.

time step. Thus, for example, $u^{n+1}_{i+1/2,j}$ represents the horizontal velocity on the right side of cell (i, j) at time $t + \delta t$.

With these definitions, [16]–[18] describing fluid-phase motion are approximated by the following finite difference equations (F.D.E's).

The r-direction momentum equation:

$$\frac{u^{n+1}_{i+1/2,j} - u^n_{i+1/2,j}}{\delta t} - \frac{r_i u^n_{i+1/2,j} u^n_{i-1/2,j} - r_{i+1} u^n_{i+3/2,j} u^n_{i=1/2,j}}{r_{i+1/2}\delta r} - \frac{u^n_{i+1/2,j-1/2} v^n_{i+1/2,j-1/2} - u^n_{i+1/2,j+1/2} v^n_{i+1/2,j+1/2}}{\delta z}$$

$$= \frac{\theta_{i,j} - \theta_{i+1,j}}{\delta r} + \frac{\mu}{\rho}\left[\frac{1}{\delta z^2}(u^n_{i+1/2,j+1} + u^n_{i+1/2,j-1} - 2u^n_{i+1/2,j}) - \frac{1}{\delta r \delta z}(v^n_{i+1,j+1/2} - v^n_{i+1,j-1/2} - v^n_{i,j+1/2} + v^n_{i,j-1/2})\right]. \quad [32]$$

The z-direction momentum equation:

$$\frac{v^{n+1}_{i,j+1/2} - v^n_{i,j+1/2}}{\delta t} - \frac{r_{i-1/2} u^n_{i-1/2,j+1/2} v^n_{i-1/2,j-1/2} - r_{i+1/2} u^n_{i+1/2,j+1/2} v^n_{i+1/2,j+1/2}}{r_i \delta r} - \frac{v^n_{i,j+1/2} \cdot v^n_{i,j-1/2} - v^n_{i,j+3/2} v^n_{i,j+1/2}}{\delta z}$$

$$= \frac{\theta_{i,j} - \theta_{i,j+1}}{\delta z} + \frac{\rho_p - \rho}{\rho} g\phi^0(1 - \Phi^n_{i,j+1/2}) - \frac{\mu}{r_i \rho \delta r}\left[r_{i+1/2}\left(\frac{u^n_{i-1/2,j+1} u^n_{i-1/2,j}}{\delta z} - \frac{v^n_{i+1,j+1/2} - v^n_{i,j+1/2}}{\delta r}\right)\right.$$

$$\left. - r_{i-1/2}\left(\frac{u^n_{i-1/2,j+1} - u^n_{i-1/2,j}}{\delta z} - \frac{v^n_{i,j-1/2} - v^n_{i-1,j+1/2}}{\delta r}\right)\right], \quad [33]$$

and the continuity equation:

$$D^{n+1}_{i,j}(u, v) = \frac{r_{i+1/2} u^{n+1}_{i+1/2,j} - r_{i-1/2} u^{n+1}_{i-1/2,j}}{r_i \delta r} + \frac{v^{n+1}_{i,j+1/2} - v^{n+1}_{i,j-1/2}}{\delta z} = 0. \quad [34]$$

These F.D.E.'s are seen to be approximations to the original partial differential equations term by term.

A cycle of time advancement consists of (1) solving the above set of F.D.E.'s for fluid movement given n-level velocities, pressure, and particle distribution and (2) using the resultant $(n + 1)$-level velocities to obtain the $(n+1)$-level particle distribution used in the next cycle.

In the first phase, fluid movement is advanced using the ingenious SMAC method. In order to understand the method, notice that the two fluid momentum equations (or their F.D.E. equivalents) may be combined after cross-differentiation to yield a pressure-independent transport equation for vorticity. This implies that if a zero pressure field ($\theta = 0$) is inserted into the momentum equations when they are solved, the resulting velocity field $(\tilde{u}, \tilde{v})$ will carry the

right vorticity although the continuity equation is yet to be satisfied. But now, if the velocity field is altered by the addition of an appropriate potential function (ψ), the altered field will carry the same vorticity, satisfy the continuity equation, and accordingly be uniquely determined—hence correct. The appropriate potential function results from the divergence of the tilde velocity field,

$$\nabla^2\psi = D(\tilde{u}, \tilde{v}). \qquad [35]$$

In the numerical solution a five-point, finite difference respresentation of this Poisson equation,

$$\frac{1}{r_i \delta r^2}[r_{i+1/2}(\psi_{i+1,j} - \psi_{i,j}) - r_{i-1/2}(\psi_{i,j} - \psi_{i-1,j})] - \frac{1}{\delta z^2}(\psi_{i,j+1} + \psi_{i,j-1} - 2\psi_{i,j}) = D_{i,j}^{n+1}(\tilde{u}, \tilde{v}) \qquad [36]$$

is solved by an SOR iteration. The resultant potential field is used to convert the tilde velocity field to the true field,

$$u_{i+1/2,j}^{n+1} = \tilde{u}_{i+1/2,j}^{n+1} - \frac{\psi_{i+1,j} - \psi_{i,j}}{\delta r} \qquad [37]$$

and

$$v_{i,j+1/2}^{n+1} = \tilde{v}_{i,j+1/2}^{n+1} - \frac{\psi_{i,j+1} - \psi_{i,j}}{\delta z}. \qquad [38]$$

This explanation is the basis of a scheme which yields a solution of the fluid dynamics in which the potential function, ψ, replaces θ, the pressure function, as one of the primary variables. Initial conditions are easily implemented by zeroing the u, v and ψ fields.

Implementation of boundary conditions requires more care. The mesh extends beyond the physical limits of the fluid, and boundary conditions are implemented by assigning fictitious variable values in the externally created "boundary cells". The boundary conditions include no-slip and free-slip velocity conditions and the condition that the gradient of ψ vanishes normal to all boundaries. Application of these conditions on the base and centerline of the cone is straightforward.

Boundary conditions are necessarily applied with less precision on the inclined boundary because it is oblique to the mesh. The handling of conditions at this boundary and other details of the fluid movement phase of the cycle of time advancement are available elsewhere (Hill 1974).

The particle-movement phase involves advancing the suspension interface. Approximately 100 point markers represent the interface and are initially located evenly along the inclined boundary. Since these markers could be identified with particles on the interface, their movement is defined by [20] and [21]. Each marker is followed in Lagrangian fashion by interpolating the current fluid velocity components at the marker position (u, v) and assuming the marker moves $u \cdot \delta t$ in the horizontal direction and $(v - W) \cdot \delta t$ in the vertical direction during the time δt.

As interface markers are repeatedly moved during a number of time steps, the even marker spacing is lost to the extent that editing is required to maintain an efficient interface representation. This is done by destroying markers in some areas and generating interpolated markers in others. Markers are also destroyed when they are sufficiently below the base.

From the interface position a particle concentration $\Phi_{i,j+1/2}^n$ is defined for each fluid cell. This concentration is defined as the fraction of the area of a mesh-size cell centered about $(i, j + 1/2)$ which is located beneath the interface. A complex algorithm was developed for this purpose.

The solution technique which has just been generally described was implemented by a computer program BESSC. Presented with system properties and solution technique

parameters, BESSC computes through a modeled sedimentation. At intervals during the sedimentation the state of the sedimentation is output via print-outs, plots, and storage on magnetic tape. The output on magnetic tape was employed by ancillary computer programs for comparison to experimental results, for interpretation in terms of an energy balance, for re-plotting, and for restarting a solution from an intermediate stage. Approximately twenty cases have been solved.

Normal execution time was 200 min on an ICL 1904A computer and 10 min on a CDC 7600 using a mesh size containing twenty fluid cells horizontally and vertically. This was a practical upper limit because the necessary computational effort increased as the cube of the mesh size. The 20×20 solutions are a reasonable approximation to the true solutions, however at least two mesh-scale aberrations are evident. Mesh-scale waves on the interface arise during early convection beneath the inclined boundary. Secondly, fluid in mesh cells at the corners where boundaries meet must remain stagnant.

COMPARISON OF THEORY AND EXPERIMENT

Settling convection

The previous illustrations of observed particle movement demonstrate an unsteady-state circulation referred to as settling convection whose presence speeds sedimentation. Solutions based on the theoretical model show settling convections with approximately the same magnitude, character, and timing as those observed. Differences are easily ascribed to experimental error and the theoretical solution technique.

This is best demonstrated by figures 10–13 which are the predicted counterparts to the experimental results shown in figures 3–6 respectively for the standard case. Predicted particle motion over 6 sec is shown by a broken line consisting of two dashes—the longer representing the particle path over the 3 sec prior to the nominal time and the shorter representing the particle path over the period from 2 to 3 sec later. The broken-line trajectory is comparable to imagined lines connecting the first four (adjacent) and the last two dots in the representation of observed motion. However, the broken line is a linear approximation based upon the velocity at the nominal time. The predicted interface is also shown in the theoretical plots. The waves in the predicted interfaces are artifacts of the numerical solution with a finite size mesh and can be mentally smoothed to the true solution. The mesh size is apparent from the steps on the inclined boundary.

Observed and predicted particle motion are combined for direct comparison in figures 14–16. Selected points in time are shown during the sedimentation of variations on the standard case.

The basic data available for comparison with model prediction consists of particle velocity measurements at various times, in various locations, and in various sedimentation systems. Each observed velocity $(\mathbf{v}_p)_{obs}$ can be compared in magnitude and direction with predicted values, $\mathbf{v} + W\hat{g}$, extracted for the given time and location in a modeling solution. The relative error between an observed and predicted particle velocity may be defined as:

$$\text{Relative error} = \frac{|\mathbf{v} + W\hat{g} - (\mathbf{v}_p)_{obs}|}{|\mathbf{v} + W\hat{g} + (\mathbf{v}_p)_{obs}|}.$$

This error term can range from zero to infinity.

Table 2 shows the average relative error at each observation time during four experimental runs. In the standard case, the average relative error was only 0.19. This low value includes experimental errors due to uncertainty in the time and place of the observation, the use of time-average experimental velocity and position, and the true settling velocity distribution of the markers. The average relative error was also this low in the runs involving particles of size II and involving the 47°-base–angle cone.

The run involving a higher particle concentration yielded a greater relative error. There are

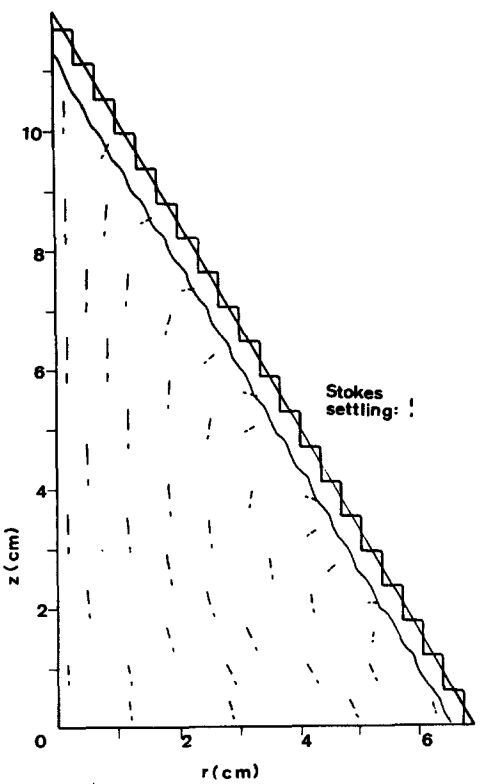

Figure 10. Settling time, 15 sec.

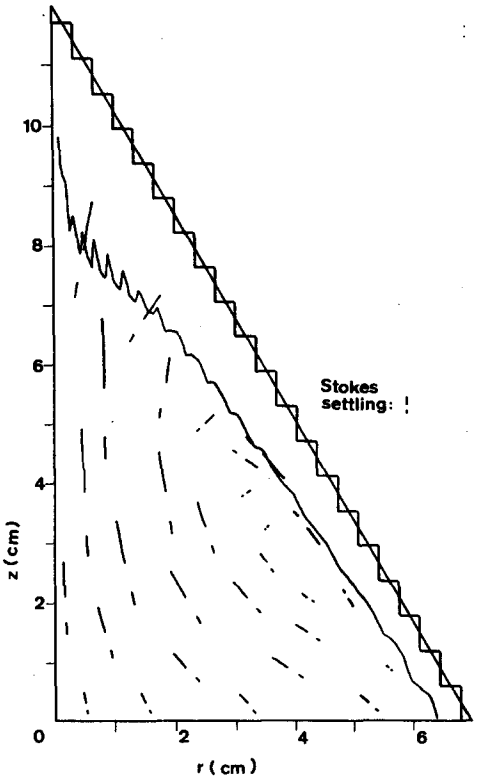

Figure 11. Settling time, 30 sec.

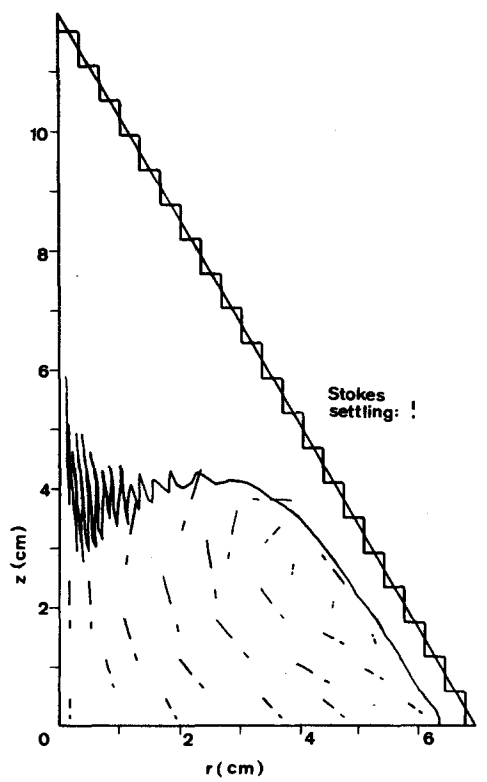

Figure 12. Settling time, 45 sec.

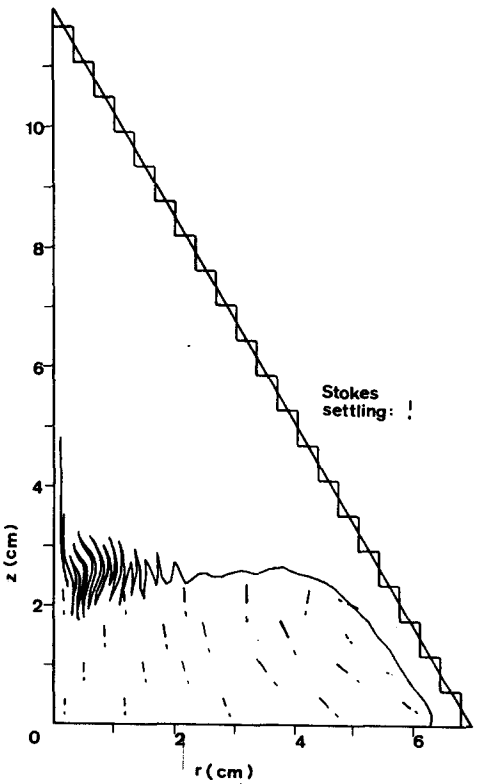

Figure 13. Settling time, 60 sec.

Figures 10–13. Interface position and particle trajectories predicted by continuum model for standard case. $N_{Gr} = 10{,}720$, $N_{Re} = 1.49$, $B/A = 1.71$.

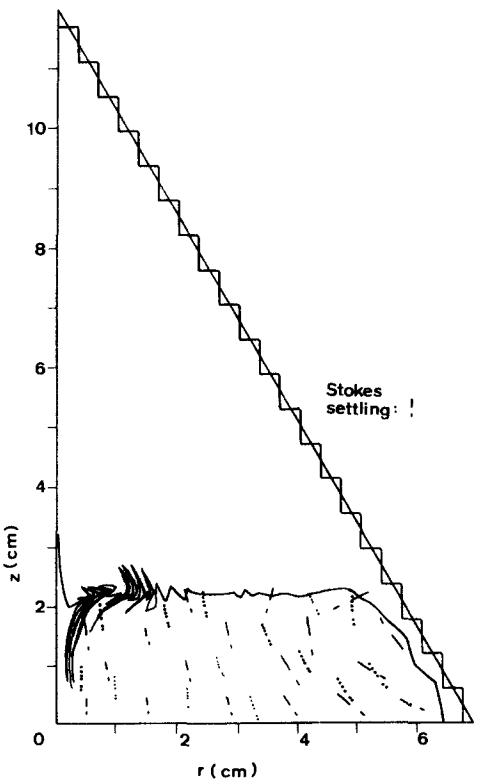

Fig. 14.

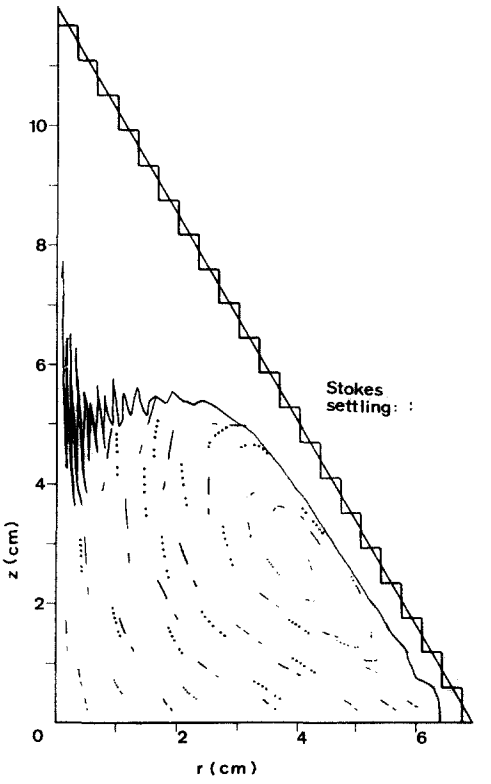

Fig. 15.

Figure 14. Comparison of observed and predicted particle trajectories for case of higher concentration than standard (0.002 volume fraction). Predicted interface also shown. $N_{Gr} = 42{,}870$, $N_{Re} = 1.49$, $B/A = 1.71$. Settling time, 60 sec.

Figure 15. Comparison of observed and predicted particle trajectories for case of smaller particles than standard (size fraction II). Predicted interface also shown. $N_{GR} = 10{,}780$, $N_{Re} = 0.811$, $B/A = 1.71$. Settling time, 60 sec.

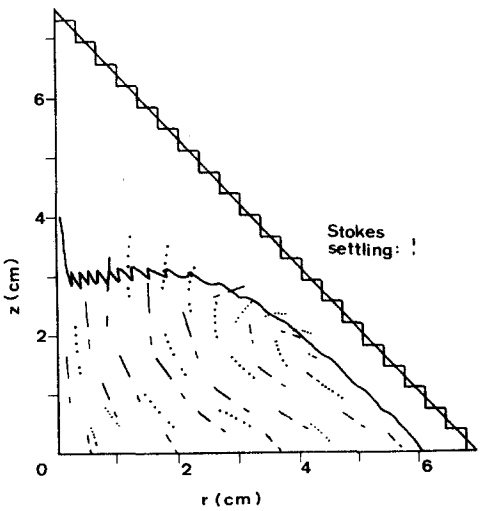

Figure 16. Comparison of observed and predicted particle trajectories for case of less acute cone than standard (cone base angle 47.0°). Predicted interface also shown. $N_{Gr} = 10{,}720$, $N_{Re} = 1.49$, $B/A = 1.07$. Settling time, 30 sec.

Table 2. Difference between observed and predicted particle velocities during four sedimentations. Entries shown as: average relative error (number of markers observed)

Run conditions		Standard	Higher conc.	Smaller part.	Less acute cone
Particle volume fraction		0.0005	0.0020	0.0005	0.0005
Particle size fraction		I	I	II	I
Cone base angle		59.7°	59.7°	59.7°	47.0°
	Time (sec)				
Average	15	0.21(62)			0.20(45)
relative	30	0.15(41)	0.42(48)	0.21(69)	0.18(41)
error	45	0.24(44)			
	60	0.26(36)	0.34(28)	0.18(40)	0.07(14)
	75	0.09(25)			
	90	0.08(12)	0.13(7)	0.22(22)	
	120			0.17(19)	
	150			0.13(9)	
	overall	0.19(220)	0.37(83)	0.19(159)	0.17(100)

two explanations for this result. Marker images in the experimental photographs were not as clear as in the other runs because the images were viewed through more "matched"-refractive-index beads.

The second explanation is that the numerical approximation to the cone at its base corners was too crude and restricted the solution. The bottom, right-hand, interior cell in the numerical mesh can contain no fluid flow because it is only open on one side. Although the driving force may be sufficient to convect particles into the bottom, right-hand cell, this is not possible in the numerical solution. Thus if the cell is large enough to restrict base coverage by the cloud, particle removal through the base is thereby limited. The solution is inexact in the higher concentration run for this reason. This limitation, which is apparent in figure 14, could be removed by using a finer mesh.

Convective velocities above the suspension interface were also examined by using substitute markers which settled relatively slowly. An aluminum dust was used which settled at a tenth of the rate of the clear standard beads with which it was dispersed at nominal concentration. The markers had a mean settling velocity of 0.0043 ± 0.0002 cm/sec. Comparison between observed movement of these markers in an otherwise standard run and predicted movement, based on the mean settling velocity (no account made for the distribution), gave an average relative error of only 0.31.

Interface movement

The comparison of observed and predicted interfaces is impaired because both appear irregular. Experimental interfaces are ill defined, particularly at early times. Location of interface positions, as shown in figure 7 for the standard case, involves extensive subjective judgement. The comparable predicted interface positions are shown in figure 17. Irregularities in these interfaces can be shown to be artifacts of the finite mesh in the numerical solution. Experimental and theoretical interfaces have the same general shapes.

At later stages of the sedimentation, the experimental interface becomes much better defined. Small scale settling convection presumably acts to smooth the interface. At these later stages experimental and theoretical interfaces match quite well. After 90 sec in the standard case the areas beneath the two interfaces match to within a few percent. Settling time was generally well predicted.

PERSPECTIVES ON THE MODEL

Limits

The theoretical lower limit to settling convection and its enhancement of sedimentation is the no-convection case of simple settling. The initial interface moves vertically downwards with the Stokes settling velocity.

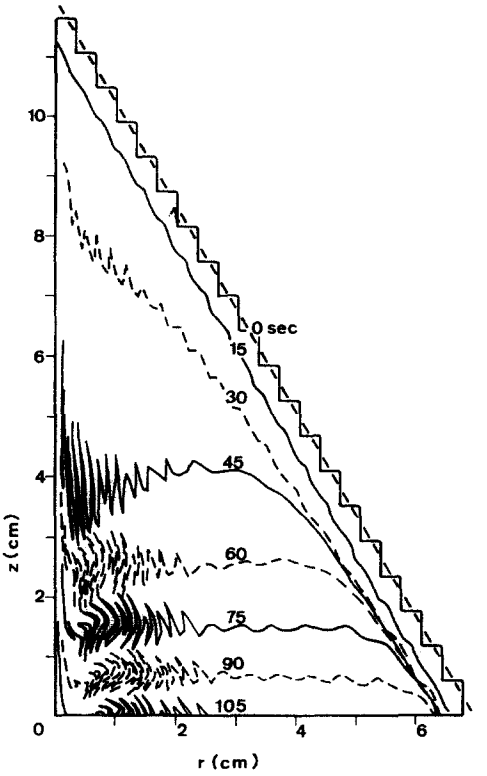

Figure 17. Interface positions predicted for the standard case.

The "PNK" theory of Ponder (1925) and Nakamura & Kuroda (1937) represents an upper limit to the enhancement of sedimentation by settling convection. The complete leveling and base coverage in this theory represents an upper limit to the rate of removal, which in the continuum model, is proportional to base coverage.

If applied to settling under a cone, the PNK theory predicts a horizontal settling interface whose height, $z(t)$, is

$$\frac{z}{B} = 1 - \sqrt[3]{\left(\frac{3Wt}{B}\right)}. \qquad [39]$$

The theory does not predict anything but this interface movement.

Solutions to the continuum model proposed here lie between the no convection and PNK limits in terms of rate of particle removal. This is illustrated in figures 20 and 21 by the time dependence of the volume still containing particles. The continuum model solution is shown for various values of N_{Re} and N_{Gr}. The limits are, however, not specific to any case but are functions solely of the normalized time, Wt/B.

The plot for the continuum model solution is a deceptively linear representation of a very non-linear solution. During the first quarter of the sedimentation in the standard case, the solution follows the no-convection limit. Settling convection increases the removal rate above this limit. For a time the removal rate is held practically constant. Later as the settling convection damps, the removal rate falls off more rapidly. Settling is completed in the standard case in about 40 per cent of the time required in the no-convection limit.

Figures 20 and 21 also show the numerical limit to the rate of particle removal when a 20×20 mesh is used. This limit corresponds to the restriction on particles convecting into the bottom, right-hand cell. By experimentation with a finer mesh it was shown that this limit was not significantly active in affecting the standard solution.

Energy

Settling convection may be profitably examined from the perspective of an unsteady-state, macroscopic, energy balance:

$$\begin{pmatrix}\text{Initially}\\ \text{available}\\ \text{potential}\\ \text{energy}\end{pmatrix} = \begin{pmatrix}\text{Remaining}\\ \text{available}\\ \text{potential}\\ \text{energy}\end{pmatrix} + \begin{pmatrix}\text{Kinetic}\\ \text{energy of}\\ \text{convective}\\ \text{flow}\end{pmatrix} + \begin{pmatrix}\text{Net viscous}\\ \text{dissipation}\\ \text{due to Stokes}\\ \text{flow}\end{pmatrix} + \begin{pmatrix}\text{Net viscous}\\ \text{dissipation due}\\ \text{to convective}\\ \text{flow}\end{pmatrix}. \quad [40]$$

Thus the potential energy lost by settling particles is converted (1) to convective kinetic energy and (2) to internal energy by the viscous dissipation of both the convective flow and flow around settling particles. The term "convective flow" represents flow on the scale of the enclosure and is exclusive of flow on the scale of individual particles. Flow on the scale of the particles does not appear in the balance because its contribution can be assumed constant in the context of the model. Effects of particle rotation and dilational forces were negligible in the balance.

The terms in the energy balance can be computed from the numerical solution of a continuum model (Hill 1974). Figure 18 shows the result of such computation for the standard case solution. Energy values are shown as fractions of the initial available potential energy, 1.52×10^{-4} joule. Again the no-convection limit is shown in which lost potential energy is identically dissipated by the Stokes flow around the settling particles.

In the continuum solution, some of the available potential energy is converted to the kinetic energy of a convective flow. The proportion of energy in this kinetic form reaches a maximum of only 0.3 per cent as shown on an expanded scale in figure 19. The kinetic energy is expeditiously dissipated by strong viscous forces. Thus, in spite of the small magnitude of kinetic energy, 23 per cent of the initial energy is eventually dissipated by convective flow.

The energy balance shows that, after sedimentation is complete, the net energy which was

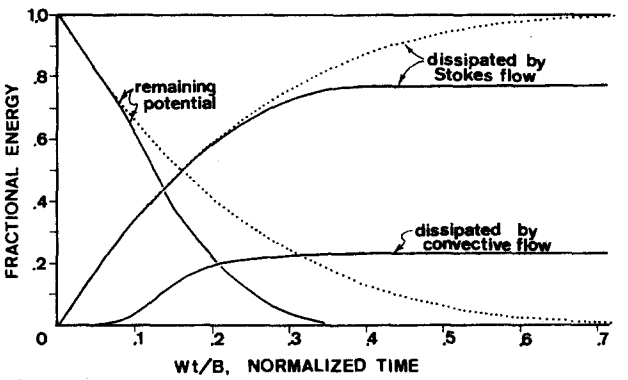

Figure 18. Energy distribution. ——, Standard case. · · · · · ·, Limit of no-convection.

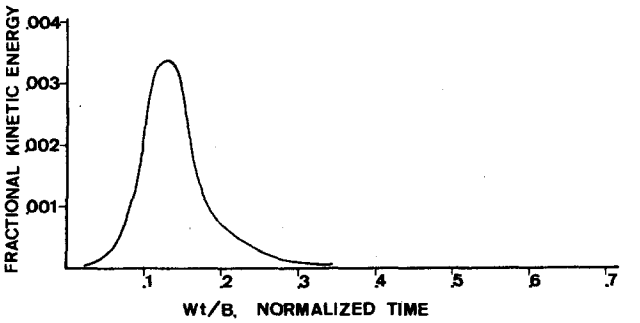

Figure 19. Kinetic energy during sedimentation of the standard case.

dissipated by convective flow must have been counterbalanced by a savings in the energy dissipated by the Stokes flow around the settling particles. Under the assumptions of the theory, this can only occur if the particles are removed more quickly as a result of the convection.

MODEL PARAMETERS

The variables affecting settling convection are best discussed in terms of dimensionless parameter groups. In the continuum model, two groups, the sedimentation Grashof number and the sedimentation Reynolds number, enter through the modeling equations. A complete set of dimensionless groups defining a problem in settling convection is formed by supplementing these two groups with those groups entering through boundary and initial conditions. For batch sedimentation in a cone, one additional group enters in defining the inclined boundary. This is the tangent of the cone base angle, i.e. B/A if B is the height and A is the radius of the base of the cone.

Sedimentation Grashof number

The sedimentation Grashof number, $[B^3 g\rho(\rho_p - \rho)\phi^0]/\mu^2$, represents the significance of gravitational forces relative to viscous forces in any convective flow. The Grashof number was varied in experimental and theoretical studies by adjusting the initial particle concentration, ϕ^0.

A Grashof number of zero corresponds to the no-convection limit. As the Grashof number increases from zero a convection appears late in the sedimentation at which time the convection can be effectively centered away from strong viscous dissipation by the enclosure walls. As N_{Gr} increases further, settling convection acts earlier during the sedimentation toward leveling non-horizontal, suspension interfaces. The convection becomes more forceful and more effective in leveling the interface early in the sedimentation process. As $N_{Gr} \to \infty$, the PNK limit of a uniformly horizontal interface is approached. Figure 20 illustrates the effect of N_{Gr} in swinging particle removal from one possible limit to the other.

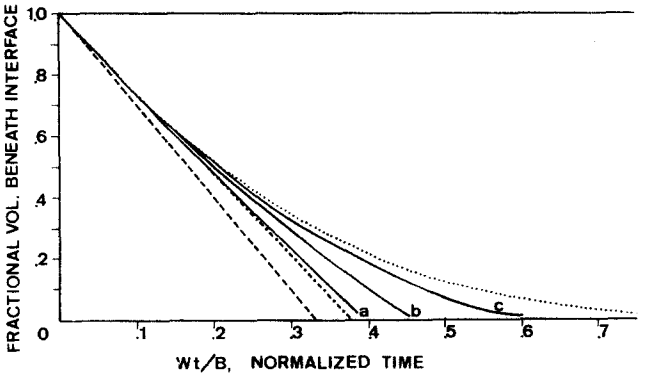

Figure 20. Effect of N_{Gr} on volume beneath interface. – – –, PNK limit ($N_{Gr} \to \infty$). ——, (a) Standard case: $\Phi^0 = 0.0005$, $N_{Gr} = 10{,}720$. ——, (b) $\Phi^0 = 0.0001$, $N_{Gr} = 2150$. ——, (c) $\Phi^0 = 0.00002$, $N_{Gr} = 430$. · · · · · ·, Limit of no-convection ($N_{Gr} \to 0$). – · – · –, Numerical limit using a 20×20 computing mesh.

Sedimentation Reynolds number

The sedimentation Reynolds number, $(BW\rho)/\mu$, represents the significance of inertial forces relative to viscous forces in any convective flow. The Reynolds number was varied in experimental and theoretical studies by adjusting the particle settling velocity, W.

Note from its definition that as Reynolds number increases the sedimentation time decreases. Processes at varying N_{Re} are comparable in terms of normalized time, Wt/B, rather than real time. In normalized time the processes will be compared at about the same stage of particle removal. The comparison is identical at the limits.

The Reynolds number is equivalent to a ratio of normalized time, scaled for vertical sedimentation, to the dimensionless time, T, used in the dimensionless form of the continuum equations. T was scaled for viscous damping. Thus the higher the N_{Re}, the more important is the "inertia" of vertical particle sedimentation relative to the viscous dissipation of a convective flow. Convection acts later during the sedimentation process (later in normalized time) to level the suspension interface. A larger horizontal imbalance in concentration accumulates, and the convection is driven to a greater magnitude.

Figure 21 shows that the later and more forceful convection which occurs at higher N_{Re} is less effective in speeding particle removal. Less energy is dissipated by settling convection because the convection occurs over a shorter real time and, since it also occurs at a later stage in the sedimentation, the convection is centered away from the cone walls.

The no-convection limit is approached as $N_{Re} \to \infty$; settling occurs before any settling convection can occur. The PNK limit is approached as $N_{Re} \to 0$; settling convection achieves substantially complete interface leveling at all times. These limiting solutions may occur outside the bounds of assumptions in the theory such as the assumption of laminar flow.

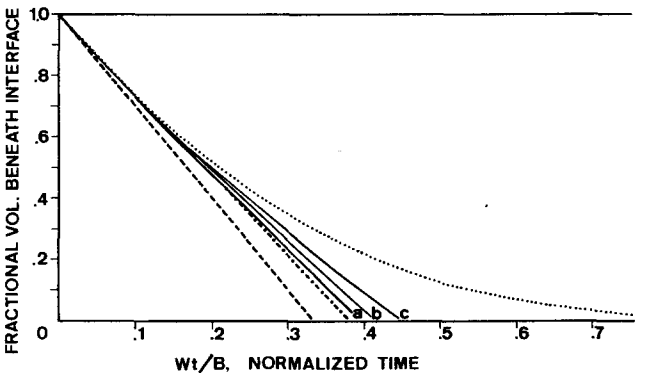

Figure 21. Effect of N_{Re} on volume beneath settling interface. – – –, PNK limit ($N_{Re} \to 0$). ——, (a) Standard case: $W = 0.046$ cm/sec, $N_{Re} = 1.49$. ——, (b) $W = 0.100$ cm/sec, $N_{Re} = 3.24$. ——, (c) $W = 0.200$ cm/sec, $N_{Re} = 6.28$. · · · · · ·, Limit of no-convection ($N_{Re} \to \infty$). – · – · –, Numerical limit using a 20×20 computing mesh.

Enclosure geometry and scale

The tangent of the cone base angle, B/A, is the third and final dimensionless parameter to appear in settling convection theory. B/A was varied in a theoretical study via A, the base radius, while B remained constant.

There are two effects of varying B/A in this way. First note that vessel volume decreases with A, and viscous forces restrict convection more strongly. In the limit of $B/A \to \infty$ there is no convection.

The second effect to note is that when cones and the sedimentation interfaces within are of quite different horizontal and vertical dimensions, the most effective convective flow pattern is oblong. The oblong flow pattern dissipates energy more quickly than would a more circular flow pattern of similar magnitude of flow. In an acute cone this effect may be reduced as convection levels the interface and the flow becomes more circular. In an obtuse cone, however, leveling will only cause the convective flow to become more horizontally oblong. Thus in the limit of $B/A \to 0$, there is no convection.

The above two effects tend to counterbalance each other so that an optimum cone angle exists for an acute cone. The optimum is generally a function of N_{Re} and N_{Gr}.

From the viewpoint of design the effect on vessel scale, B, is also of particular interest. The effect is not immediately clear because increasing B (with B/A and other primary variables held constant) increases effectiveness through N_{Gr} but decreases this effectiveness through N_{Re}. The important effect of B is its effect on the ratio N_{Gr}/N_{Re} in [2]. This ratio represents the

significance of gravitational forces to inertial forces in any convective flow. An increase in B increases the ratio as B^2, and thus a given horizontal imbalance in particle concentration is removed more quickly relative to a normalized time scale of sedimentation. Settling convection occurs relatively earlier and to a greater and more effective degree in larger scale cones.

CONCLUSIONS AND SIGNIFICANCE

Increased sedimentation rates observed in enclosures without a single, horizontal upper surface result from a naturally occurring convection. In systems with only 0.0005 volume fraction particles, velocities of this "settling convection" exceed the normal particle settling velocity by an order of magnitude.

Assuming that settling convection is caused by momentum transfer from particles to fluid, a mechanistic model is developed based upon continuum fluid dynamics. Fluid motion satisfies a continuity equation and a Navier–Stokes equation to which is appended a term representing momentum transfer from settling particles. This Boussinesq-like transfer term is linear in particle concentration. The equations of particle motion may be interpreted to show that particles move with a constant velocity relative to the fluid and are contained at a uniform and constant concentration beneath a sharp interface.

An experimental study of the sedimentation beneath a cone of dilute suspensions of monodisperse particles in a viscous, incompressible and Newtonian fluid was used to verify the model. Experimental runs with varying particle settling velocity, particle concentration, and conical geometry matched model predictions which were based solely upon basic physical properties. The match was very good in terms of settling time and the convection velocity field.

The model shows that sedimentation beneath a cone is dependent upon only three dimensionless groups—a sedimentation Grashof number, $N_{Gr} = B^3 g\rho(\rho_p - \rho)\phi^0/(\mu^2)$; a sedimentation Reynolds number, $N_{Re} = BW\rho/\mu$; and the tangent of the cone base angle, B/A. The case of vertical settling with no convection is approached as $N_{Gr} \to 0$, $N_{Re} \to \infty$, $B/A \to 0$ or $B/A \to \infty$. The most rapid sedimentation, the case where the convection sustains a horizontal interface, is approached as $N_{Gr} \to \infty$ or $N_{Re} \to 0$.

When N_{Gr} increases, settling convection acts more quickly toward leveling a given non-horizontal, suspension interface. Convection occurs earlier and is more forceful.

When N_{Re} increases, both vertical settling and settling convection occur faster, but vertical settling proceeds to a greater extent before settling convection occurs. As N_{Re} increases within the range of practical interest settling convection is more forceful.

The continuum model is the first model of settling convection to have a mechanistic basis. This mechanism, particle momentum-transfer to the fluid, wholly accounts for strong convection in a dilute system. Since the mechanism becomes more forceful in more concentrated systems, the mechanism is also of prime importance in these systems.

Acknowledgements—Financial support for this work was provided by the governments of the United States and the United Kingdom through a Fulbright–Hays Grant, by the Armstrong Cork Company, by Carnegie–Mellon University and by Loughborough University of Technology (England). Mr. B. Scarlett, Senior Lecturer, advised in this work, the results of which were submitted for the degree of Doctor of Philosophy of Carnegie–Mellon University.

REFERENCES

AMSDEN, A. A. & HARLOW, F. H. 1970*a* The SMAC method: a numerical technique for calculating incompressible fluid flows, Report LA-4370, Univ. Calif., Los Alamos Sci. Lab., Los Alamos, N.M.

AMSDEN, A. A. & HARLOW, F. H. 1970*b* A simplified MAC technique for incompressible fluid flow calculations. *J. Comp. Phys.* **6**, 322–325.

BOYCOTT, A. E. 1920 Sedimentation of blood corpuscles. *Nature* **104**, 532.

BRADLEY, W. H. 1965 Vertical density currents. *Science* **150**, 1423–1428.

COUTTS, J. & CROWTHER, E. M. 1925 Source of error in the mechanical analysis of sediments by continuous weighing. *Trans. Faraday Soc.* **21**, 374f.

GRAHAM, W. & LAMA, R. 1963 Continuous thickening in an inclined thickener. *Can. J. Chem. Engng* **41**, 162–165.

HILLS, W. D. 1974 Boundary-enhanced Settling due to Settling Convection. Ph.D. Thesis, Carnegie–Mellon University, Pittsburgh, PA.

KAST, W. 1960 Die störung der sedimentation analyses durch das unströmen vor Körpern in sedimentationeagefass. *Staub* **20**, 205f.

KINOSITA, K. 1949 Sedimentation in tilted vessels (1). *J. Coll. Sci.* **4**, 525–536.

LUNDGREN, R. 1927 *Acta Med. Scand.* **67**, 63f.

LUNDGREN, R. 1928 *Acta Med. Scand.* **69**, 405f.

NAKAMURA, H. & KURODA, K. 1937 *Keijo, J. Med.* **8**, 256f.

OLIVER, D. R. & JENSON, V. G. 1964 The inclined settling of dispersed suspensions of spherical particles in square section tubes. *Can. J. Chem. Engng* **42**, 191–195.

PEARSE, 1921 Report on Industrial Wastes from Stockyards and Packington, Chicago, II, 137.

PONDER, E. 1925 On sedimentary and rouleaux formation. *Q. J. exp. Physiol.* **15**, 235–252.

SOO, S. L. 1967 *Fluid Dynamics of Multiphase Systems.* Blaisdell, Waltham, MA.

STRONG, J. 1938 *Procedures in Experimental Physics.* Prentice-Hall, New York.

VOHRA, D. K. & GHOSH, B. 1971 Studies of sedimentation in inclined tubes. *Ind. Chem. Engng* **13**, 32–40.

WOODWARD, D. H. 1964 Sedimentation of monodisperse polystyrene latex spheres in water. *J. Coll. Sci.* **19**, 238–244.

ZAHAVI, E. & RUBIN, E. 1975 Settling of solid suspensions under and between inclined surfaces. *Ind. Engng Chem. Process Des. Develop.* **14**, 34–41.